Article:
Wen, Y, Sobott, F and Devreese, B (2016) ATP and autophosphorylation driven conformational changes of HipA kinase revealed by ion mobility and crosslinking mass spectrometry. Analytical and Bioanalytical Chemistry, 408 (21). pp. 5925-5933. ISSN 1618-2642

https://doi.org/10.1007/s00216-016-9709-3

ATP and autophosphorylation driven conformational changes of HipA kinase revealed by ion mobility and crosslinking mass spectrometry

Running title: Mass spectrometric study of the HipAB complex

Yurong Wen[1, 2], Frank Sobott[3], Bart Devreese[2]

[1] Center for Translational Medicine, School of Life Science and Technology and Frontier Institute of Science and Technology, Xi'an Jiaotong University, Xianning West Road 28, 710049 Xi'an, Shaanxi, China

[2] Unit for Biological Mass Spectrometry and Proteomics, Laboratory for Protein Biochemistry and Biomolecular Engineering (L-ProBE), Ghent University, K.L. Ledeganckstraat 35, 9000 Ghent, Belgium.

[3] Biomolecular & Analytical Mass Spectrometry Group and UA-VITO Center for Proteomics (CFP-CEPROMA), University of Antwerp, 2020 Antwerp, Belgium;

Address reprint requests to: Bart Devreese E-mail: Bart.Devreese@Ugent.be ; Fax: +32 9 264 53 38 Tel: +32 9 264 52 73. Unit for Biological Mass Spectrometry and Proteomics, Laboratory for Protein Biochemistry and Biomolecular Engineering (L-ProBE), Ghent University, K.L. Ledeganckstraat 35, 9000 Ghent, Belgium.

Abstract

Toxin Antitoxin systems are genetic modules involved in a broad range of bacterial cellular processes including persistence, multidrug resistance and tolerance, biofilm formation and pathogenesis. In type II toxin antitoxin systems, both the toxin and antitoxin are proteins. In the prototypic *Escherichia coli* HipA-HipB module, the antitoxin HipB forms a complex with the protein kinase HipA, and sequesters it in the nucleoid. HipA is then no longer able to phosphorylate glutamyl tRNA synthetase and this prevents the initiation of the forthcoming stringent response. Here we investigated the assembly of the *Shewanella oneidensis* MR-1 HipA-HipB complex using native electrospray ion mobility mass spectrometry and chemical crosslinking combined with mass spectrometry. We revealed that the HipA autophosphorylation is accompanied with a large conformational change and confirmed structural evidence that *S. oneidensis* MR-1 HipA-HipB assembly is distinct from the prototypic *E. coli* HipA-HipB complex.

Introduction

Shewanella oneidensis MR-1 is a gram negative bacterium that is widely studied for its potential application in bioremediation, microbial fuel cells and nanotechnology [1-3]. All of these applications are highly dependent on the capacity of this bacterium to form biofilms. We previously reported a role for the SO0706 gene in *S.oneidensis* MR-1 biofilm formation. Indeed, transposon mutagenesis of this gene led to a 50% decrease of biofilm formation [4]. The SO0706 gene encodes a protein that is homologous to the HipA toxin, a protein kinase from *Escherichia coli* (28% identity). HipA was reported to belong to the Serine/Threonine kinase family with similarity to the PI3/4 kinase super family. It can be partially autophosphorylated *in vivo* or upon incubation with ATP and Mg^{2+} *in vitro* [5, 6]. While it was originally believed that HipA halts ribosomal activity by phosphorylating elongation factor Tu (EF-Tu) [7, 8], it was recently established that its natural substrate is actually glutamyl-tRNA-synthetase. By phosporylating this enzyme at its ATP binding site, uncharged glutamyl tRNA accumulates and the stringent response is activated [9, 10]. The *hipA* gene forms an operon with *hipB*, which codes for a labile antitoxin that neutralizes HipA activity by forming a HipAB complex. HipB is a helix-turn-helix motif containing DNA-binding protein that mediates interactions with operators located upstream of the HipAB operon to reduce HipA expression [7]. Recently, based on X-ray crystallographic data, we demonstrated a distinct ternary assembly of the *S. oneidensis* HipAB with its operator DNA [6]. Moreover, we showed that phosphorylated HipA binds with higher affinity to the HipAB:DNA complex, whereas it was believed that phosphorylation would lead to release of HipA from the complex in *E.coli*. The structural differences between the *S. oneidensis* and *E.coli* HipAB-DNA complex formation indicated that mechanical regulation of HipAB toxin antitoxin (TA) system in bacterial persistence may be diverse and still elusive [6].

We here provide the results of a set of mass spectrometric experiments involving ion mobility mass spectrometry (IM-MS) and chemical crosslinking experiments that give further insights in the *S.oneidensis* MR-1 HipA-HipB assembly, its regulation and the HipA kinase mechanism. Firstly, IM-MS results indicated that HipA has three different conformational states, i.e. apoHipA, Mg^{2+}-ATP bound HipA and phosphorylated HipA (pHipA). We show that binding of Mg^{2+}-ATP drives the HipA conformational change required for its autophosphorylation. Secondly, we confirm that the *S.oneidensis* MR-1 HipA-HipB assembly is distinct from the homologue from *E.coli* as demonstrated by IM-MS and crosslinking mass spectrometry (XL-MS) studies. Finally, our XL-MS data give further support to the pLoop ejection as a direct consequence of HipA autophosphorylation.

Experimental procedures

Materials

All chemicals were obtained from Sigma-Aldrich (St-Louis, MO, USA) unless otherwise stated. LC-MS grade solvents were from Biosolve (Valkenswaard, NL).

Preparation of protein and protein-DNA complex samples

S.oneidensis MR-1 HipA, HipAD306Q, HipB proteins with an N-terminal His-tag were expressed in *E.coli* BL21(DE3) cells using the pET15b expression vector (EMD Biosciences, San Diego, CA, USA). Stable overexpression of the target proteins was obtained by inducing the cultures for 1h (HipA) or 4h (HipB) with 1mM isopropyl β-D-1-thiogalactopyranoside (IPTG) (Duchefa Biochemie, Haarlem, NL) when cultures were grown to an OD600 of 0.6-0.7 in LB medium supplied with carbenicillin (100µg/ml; P212121, Ypsilanti, MO, USA) at

37ºC. Detailed overexpression and purification protocols were previously described [6]. The double stranded operator DNA was obtained from annealing two single primers 5'-ATTAGGTGTACTTATCTACACTTTTT-3', 5'-AAAAAGTGTAGATAAGTACACCTAAT-3' (obtained from Integrated DNA Technologies, Leuven, BE). The HipAB and HipB:DNA complex were formed by mixing proper ratios and subsequently purified by gel filtration on a Hiload 16/60 Superdex 200 chromatography column using an Akta Purifier system (GE Healthcare, Diegem, BE). The concentrations of the samples are determined with a Nanodrop instrument (Thermo Fisher Scientific, Waltham, MA, USA).

Electrospray ionization ion mobility mass spectrometry analysis

Purified samples with a protein concentration of 10-20μM were buffer exchanged against 100-200mM ammonium acetate (pH 7) using Micro Biospin 6 columns (Bio-Rad, Hercules, CA, USA) just prior to MS analysis. The Mg^{2+}-ATP HipA complex was obtained by adding 5mM ATP and 10mM $MgCl_2$ to the buffer exchanged sample just before the MS measurement. The traveling wave ion mobility MS measurements were performed on a q-IMS-TOF instrument (Synapt G1 HDMS, Waters, Manchester, UK) equipped with a Nanomate electrospray ionization source (Advion, Ithaca, NY, USA). The samples were sprayed using a capillary voltage of 1.65-1.75kV using the type D nano-ESI chip (Advion, Ithaca, NY, USA). The IM separator, filled with Nitrogen, was pressurized at 0.5 mbar. The applied instrumental parameters were: sample cone 80V, bias 35V, Trap CE 10V, Transfer CE 4V, ion mobility wave velocity 400m/s, wave height 12V, transfer wave velocity 140m/s, wave height 5V. Ions underwent TOF analysis with m/z range from 1500 or 2000 to 8000. The TOF tube vacuum pressure maintained at around 9.5×10^{-7} mbar. Denatured myoglobin ions were used for the Nitrogen CCS calibration and all the other instrument parameters were

tuned by following the protocol reported by Ruotolo et al. [11]. The CCS calibration curve generated from DriftScope software is shown in supplementary material (Figure S1). The experimental CCS value was obtained from triplicate measurements using the same IM parameters. All the data were analyzed using Masslynx V4.1 and DriftScope V2.3 (Waters) with minimal smoothing and background subtraction. For comparison with the experimental CCS values, the PA CCS value was multiplied by a scaling factor of 1.14 [12].

The theoretical CCS of *S.oneidensis* MR-1 and *E.coli* HipAB assemblies were calculated by applying the Projection Approximation (PA) mode [12] using the PDB data files for *E.coli* (3DNV, 3FBR and 3TPE) and *S.oneidensis* MR-1 (4PU3, 4PU5 and 4PU7) containing the atomic resolution crystal structures of the different subunits and DNA complexes [6-8].

Chemical crosslinking proteolysis and LC-MS analysis of crosslinked peptides

We selected Bis[sulfosuccinimidyl] suberate (BS3, Thermo Scientific Pierce, Rockford, IL, USA) for the crosslinking experiments. We prepared a stock concentration of 100mM or 200mM BS3 in water. We then optimized crosslinking conditions by applying different BS3 concentrations (0mM, 0.5mM, 1mM, 2mM and 5mM) and incubation time (15min, 30min, 45min, 60min and 120min). Incubation at both 4°C and at room temperature was also compared. The crosslinking efficiency was evaluated by SDS-PAGE. Based on this optimization, it was decided to add 1mM or 2mM of BS3 to the purified protein or protein complex and the mixture was incubated at room temperature for 45-60min. The reaction was quenched by the addition of Tris buffer pH7.0 to a final concentration of 50mM. The sample was subsequently digested overnight with trypsin (Porcine sequencing grade, Promega, Madison, MA, USA) at 37 °C using an enzyme to protein ratio of 1:20. The sample buffer was exchanged to 50mM NH_4HCO_3 using a Superdex peptide PC 3.2/30 column which also

allowed to enrich the larger and crosslinked peptides. The fractions that eluted between 0.9-1.5 ml of elution buffer were pooled, dried and dissolved using 0.1% formic acid aqueous solution prior to LC-MS analysis. The digestion mixtures were analyzed by nanoESI LC-MS/MS. Peptides were separated using an Agilent 1200 HPLC (Agilent, Santa Clara, CA, USA) at a flow rate of 300nL/min. A C18 Acclaim PepMap300 5µm (Thermo Scientific Dionex, Sunnyvale, CA, USA) column was used to trap the peptides followed by separation on a C18 Acclaim PepMap100 (3µm) 75µm×250mm column (Thermo Scientific Dionex). Peptides were eluted with a gradient of acetonitrile. Buffer A contained 0.1% formic acid in water and buffer B was 0.1% formic acid in acetonitrile. The applied gradient was: 2%B to 10%B in 10min, 10%B to 40%B in 30min, 40% to 80% in 10min, and 80% to 2% in 5min. The column outlet was directly interfaced to a Nanomate electrospray source (Advion) equipped with D-chips connected to an LTQ-FT Fourier transform ion cyclotron resonance Mass spectrometer (Thermo Fisher Scientific). Data dependent analysis was carried out using a resolution of 100,000. MS spectra were acquired over an m/z range of 150-2000 with a charge filter above 1 and the 10 highest peaks were submitted to MS/MS scans using threshold energy of 35V for collision induced dissociation (CID). The chemical crosslink data analysis was performed using the pLink program [13].

Results and Discussion

HipA has three different detectable conformational states: apoHipA, Mg-ATP bound HipA, phosphorylated HipA

We purified the *S.oneidensis* MR-1 HipA, produced as a recombinant protein in *E. coli*. The protein is unstable under denaturing condition (50%ACN, 0.1%FA), and we could not obtain an electrospray ionization mass spectrum when the protein was dissolved at low pH because the protein precipitated. However, at pH 7, we could obtain good quality native electrospray

mass spectrometry data and we investigated the protein by ion mobility MS (IM-MS) to further characterize its molecular shape. Surprisingly, ion mobility analysis of freshly purified recombinant HipA revealed two distinct conformational populations (Figure 1a). The two populations (ATDs) from the gas phase separation were further extracted using Driftscope analysis (Table 1). The mass of one conformational form corresponded well to the theoretical mass of the HipA protein (50767.6±5.3 Da). The mass of the form that moved faster in the ion mobility device was slightly higher (50878.1±18.8 Da), and the mass difference could correspond to a phosphorylation in addition to binding a small alkali metal like Mg^{2+}. It is previously reported that also *E.coli* HipA purification results in a partially phosphorylated population which was considered to be the inactive form indicating that phosphorylation of the enzyme results in growth arrest reversion [8]. The sample used for this mass spectrometry experiment was from the same batch that was also used for determination of the crystal structure of the HipAB-DNA complex by X-ray diffraction analysis [6] . We previously performed a tryptic digest of this sample and analyzed the resulting peptides by LC-MS and found that recombinant HipA is a mixture of phosphorylated HipA (pHipA) and non-phosphorylated HipA (apoHipA). These data further indicated that there is around 5-8 % of pHipA that is phosphorylated at Ser147 [6].

In some preparations of the recombinant HipA, we observed that the phosphorylated form was nearly absent. When analyzing these samples using IM-MS, only one population was observed indicating that the mobility difference is a direct consequence of the phosphorylation (Figure 1b). Not surprisingly, phosphorylation of HipA results in a slightly shifted Gaussian distribution which can be explained by a single positive charge reduction. The drift time of pHipA and apoHipA 13^{+} ions is around 9.6ms and 13.4ms, respectively, which corresponds to a collisional cross section (CCS) difference of almost 950$Å^2$ between these 2 forms (Figure 1d). It should be mentioned that phosphorylation of S147 leads to an

additional conformational change through pLoop ejection [6]. As a matter of fact, based on the atomic resolution structure, this would lead to an increase of CCS of only 52 $Å^2$. Our instrument does not possess the IM resolution (10-15 for Synapt G1) to distinguish such a small conformational change. The change in CCS that we observe can thus not be explained by the presence of the phosphate group alone, and suggests that pHipA has a more compact conformation compared to apoHipA. In addition, the ATD peak width (7ms in apoHipA (13+ ion) vs 3ms for HipA (13+)) could indicate that apoHipA exists in multiple conformations (Figure 1a and 1c) and is thus flexible. Structural flexibility compromises protein crystallization and could explain why we obtained only X-ray diffracting crystals from the phosphorylated form even when it coexisted with the apo form.

We further analyzed the effect of binding of Mg^{2+}-ATP on the HipA conformation. Freshly purified HipA was incubated in a pH neutralized buffer containing 5mM ATP and 10mM $MgCl_2$. The ion mobility shift compared to apoHipA indicates formation of the Mg^{2+}-ATP complex to HipA which causes a shift to a more compact conformation with a CCS similar as for pHipA (Figure 1d) (Table 1, Supplementary Table S1). The CCS represents also a value for the solvent accessible surface area (SASA) in a globular protein when corrected for the molecular weight of the protein [14]. The SASA per Da of the apoHipA decreases from 0.098 $Å^2$/Da to 0.073 $Å^2$/Da upon the Mg^{2+}-ATP binding. Conformational change induced by ligand binding is a phenomenon that has been observed in several other ion mobility mass spectrometry experiments [15, 16]. More specific, nucleotide dependent conformational changes in proteins with ATPase activity are well described [17] and illustrated by ion mobility MS recently [18]. We observed also some oligomeric HipA possibly due to the Mg^{2+} and concentration effect. There is so far no evidence for a physiological role for dimeric HipA. However, autophosphorylation of HipA involves an intermolecular transfer of a phosphate group from one HipA molecule to another [8], requiring the direct contact between

two HipA molecules with low affinity. Analysis of the tryptic digest of this sample by LC-MS indicated that after incubation with ATP and Mg^{2+}, the relative amount of pHipA increased up to approximately 45-50% of the total HipA [6]. Crystal structure analysis indicated that the link between the C-terminal and N-terminal domains of HipA could be flexible and that there are five loops between those two domains involved in the ATP and Mg^{2+} binding to HipA [6]. The large conformational change represented by this difference in ion mobility is explained by considering that those five loops form a pocket that could pull together the N- and C-terminal domains in order to tightly anchor the Mg^{2+}-ATP binding, hence resulting in a substantial conformational change similar to the one observed in many kinases. Therefore, we conclude that the conformational change between the apoHipA and Mg^{2+}-ATP binding HipA results in an intermediate conformation state which serves for the HipA phosphorylation (Figure 1e).

Characterization of HipA, HipB and their operator DNA interactions by ion mobility mass spectrometry reveals a distinct assembly with respect to *S.oneidensis* MR-1 and *E.coli* HipAB complexes

hipA and its upstream linked gene *hipB* form a toxin-antitoxin module which is recognized as a major factor involved in persistence [19]. HipB is a Helix-Turn-Helix (HTH) DNA-binding protein that functions as the antitoxin. It neutralizes HipA activity by forming a complex sequestering HipA in the nucleoid following binding to the operators upstream of the HipAB TA operon. Formation of this complex suppresses the transcription of the *hipA* gene [7, 8]. Here, an IM-MS approach was applied to investigate the assembly between Mg^{2+}-ATP-HipA, HipB and its operator DNA. Native ESI analysis confirmed that HipB is a dimer with molecular weight 21838.6±1.1 Da (Figure S2). Similarly, it was determined that this dimer interacts with 2 molecules of HipA forming a $HipA_2B_2$ heterotetramer with molecular weight

127940.2±46.9 Da (Figure 2a). Several other species including the HipB dimer, Mg^{2+}-ATP-HipA monomer, Mg^{2+}-ATP-$HipAB_2$ and Mg^{2+}-ATP-$HipA_2B_2$ were nicely separated in the IM mode (Figure 2b). Additionally, we also performed ESI-MS analysis on HipB in complex with a single operator DNA showing that the $HipB_2$ dimer can interact with a single operator DNA fragment (Figure 2c). We also tested interaction with a DNA fragment containing 2 operator sites showing binding to 2 $HipB_2$ dimers (data not shown). In the HipAB operon, there are 4 identical palindromic operators equally separated by 34bp which may involve 4 $HipB_2$ dimer molecules binding. Whether those 4 operators act cooperatively is still elusive.

To gain more insight into the HipA and HipB assembly, the CCS values were experimentally determined. The experimental CCS fits well to the theoretical CCS generated using the PA model from the *S.oneidensis* MR-1 crystal structure data, with a small deviation of 2-4%. The theoretical CCS value for the HipAB complex of *E.coli* is quite different, reflecting the distinct structural assembly of both complexes [6].

The experimental CCSs of the different proteins and assemblies are well correlated in a linear relationship with their respective molecular weight (Figure 2d). Such a relationship is indicative for an extended, linear arrangement of building blocks as represented by the structural assembly of the complez [11].

Probing the HipA kinase conformational changes upon phosphorylation using chemical crosslinking

Chemical crosslinking combined with mass spectrometry was used to further probe the assembly of the *S.oneidensis* MR-1 HipA-HipB TA complex. After crosslinking the protein or protein complex using BS3, tryptic peptides were generated and analyzed using LC-MS on a high resolution FT-ICR MS instrument. Data were analyzed using the pLink software

254 which revealed 6 crosslinked peptides, including both inter- and intra-crosslinked peptides
255 (Table 2).

256 The spacer length of the BS3 crosslinker is 11.4Å and an efficient crosslink distance between
257 two lysine residue Cα atoms is reported to be approximately 5-35Å [13, 20, 21]. Distance
258 restraints are generated and nicely fit the values reported for BS3 crosslinkers (Figure 3a). It
259 is noteworthy that two distinct crosslinked sites (K35 and K64) were observed at the N
260 terminus of HipB, which could reflect the flexibility of the HipB N terminal region. The
261 distance of the intermolecular crosslink between HipA and HipB is somewhat at the limit of
262 the method, but it should be realized that the figure is derived from the HipAB-DNA complex,
263 and some more structural flexibility is expected when no DNA is bound. Surprisingly, when
264 we applied the chemical crosslinking approach to pHipA, an additional crosslinked peptide
265 was observed between K143 and K264. The MS/MS spectrum of this crosslinked peptide was
266 highly conclusive as most of the peaks could be assigned (Figure 3b). K143 is positioned
267 inside the reported phosphorylation loop (pLoop) of which repositioning is crucial for the
268 modulation of the kinase activity of HipA. Interestingly, this crosslink was not observed in
269 the HipA D306Q mutant that was reported not to undergo phosphorylation. Indeed, based on
270 data from the crystal structure of pHipA and the AMPPNP bound HipA (unphosphorylated),
271 the distance observed between K143 and K264 are 18.6Å and 40.3Å respectively (Figure 3c).
272 Without the phosphorylation, those two residues are too far away to be crosslinked. Moreover,
273 they are separated by a helix in HipA bound to the ATP-mimicking compound AMPPNP.
274 This indicates that the K143 and K264 crosslinked peptide observed from the pHipA
275 describes the phosphorylation pLoop conformational change which we could not observe
276 using ion mobility experiments.

277

Conclusion

Mass spectrometry combined with ion mobility measurements and chemical crosslinking is a powerful tool for the study of protein dynamics. In this study, three different conformations of recombinant HipA were observed in ion mobility MS experiments, indicating that the HipA kinase undergoes a large conformational change upon binding Mg^{2+}-ATP followed by p-loop ejection upon autophosphorylation. ESI-IM-MS also allowed probing of the weak non-covalent protein-protein interaction: the observation of dimeric HipA upon ATP and Mg^{2+} could reflect the trans-autophosphorylation state between two HipA molecules. Furthermore, the HipA kinase activity loop ejection mechanism was characterized through the distance restraint information generated by the chemical crosslinking mass spectrometry approach. The native ion mobility mass spectrometry data represent good correlations with the atomic resolution models revealed by X-ray crystallography and revealed a distinct assembly between *E.coli* and *S.oneidensis* MR-1 HipAB and their DNA binding structure.

Hence, the successful characterization of the *S.oneidensis* MR-1 HipA-HipB assembly and mechanism through combination of IM-MS and XL-MS established an example of gathering information on macromolecular assembly using an integrated MS approach. Toxin-antitoxin systems are mostly linked with intrinsically disordered domains or protein such as the phd-doc system [22]. Unquestionably, adding MS to an integrative structural biology approach in the study of TA systems can complement the crystallography and provide substantial additional information for non-crystallizing intermediates and to reveal transient interactions. Recently, these mass spectrometry approaches were summarized to be applicable in pharmaceutical drug discovery and development in applications to study the conformational transition and protein ligand screening [23, 24]. The toxin-antitoxin systems are proposed as an attractive target for next generation antimicrobial drug discovery, which may aid in the

302 fight to major challenges under current antibiotic treatment such as persistence, multidrug
303 tolerance and multidrug resistance etc [25-27]. The successful probing of the conformational
304 change between the HipA with its ligand binding and post-translational modification revealed
305 the potential of the MS-based approach in the investigation of protein ligand complexes and
306 can further lead to the pharmaceutical exploitation of the TA system as an antimicrobial drug
307 target.

308

References

1. Hau, H.H., Gralnick, J.A.: Ecology and biotechnology of the genus Shewanella. Annual review of microbiology. 61, 237-258 (2007)

2. El-Naggar, M.Y., Wanger, G., Leung, K.M., Yuzvinsky, T.D., Southam, G., Yang, J., et al.: Electrical transport along bacterial nanowires from Shewanella oneidensis MR-1. Proceedings of the National Academy of Sciences of the United States of America. 107, 18127-18131 (2010)

3. Gorby, Y.A., Yanina, S., McLean, J.S., Rosso, K.M., Moyles, D., Dohnalkova, A., et al.: Electrically conductive bacterial nanowires produced by Shewanella oneidensis strain MR-1 and other microorganisms. Proceedings of the National Academy of Sciences of the United States of America. 103, 11358-11363 (2006)

4. Theunissen, S., De Smet, L., Dansercoer, A., Motte, B., Coenye, T., Van Beeumen, J.J., et al.: The 285 kDa Bap/RTX hybrid cell surface protein (SO4317) of Shewanella oneidensis MR-1 is a key mediator of biofilm formation. Research in microbiology. 161, 144-152 (2010)

5. Correia, F.F., D'Onofrio, A., Rejtar, T., Li, L., Karger, B.L., Makarova, K., et al.: Kinase activity of overexpressed HipA is required for growth arrest and multidrug tolerance in Escherichia coli. Journal of bacteriology. 188, 8360-8367 (2006)

6. Wen, Y., Behiels, E., Felix, J., Elegheert, J., Vergauwen, B., Devreese, B., et al.: The bacterial antitoxin HipB establishes a ternary complex with operator DNA and phosphorylated toxin HipA to regulate bacterial persistence. Nucleic acids research. 42, 10134-10147 (2014)

7. Schumacher, M.A., Piro, K.M., Xu, W., Hansen, S., Lewis, K., Brennan, R.G.: Molecular mechanisms of HipA-mediated multidrug tolerance and its neutralization by HipB. Science. 323, 396-401 (2009)

8. Schumacher, M.A., Min, J., Link, T.M., Guan, Z., Xu, W., Ahn, Y.H., et al.: Role of unusual P loop ejection and autophosphorylation in HipA-mediated persistence and multidrug tolerance. Cell reports. 2, 518-525 (2012)

9. Germain, E., Castro-Roa, D., Zenkin, N., Gerdes, K.: Molecular mechanism of bacterial persistence by HipA. Molecular cell. 52, 248-254 (2013)

10. Kaspy, I., Rotem, E., Weiss, N., Ronin, I., Balaban, N.Q., Glaser, G.: HipA-mediated antibiotic persistence via phosphorylation of the glutamyl-tRNA-synthetase. Nature communications. 4, 3001 (2013)

11. Ruotolo, B.T., Benesch, J.L., Sandercock, A.M., Hyung, S.J., Robinson, C.V.: Ion mobility-mass spectrometry analysis of large protein complexes. Nature protocols. 3, 1139-1152 (2008)

12. Benesch, J.L., Ruotolo, B.T.: Mass spectrometry: come of age for structural and dynamical biology. Current opinion in structural biology. 21, 641-649 (2011)

13. Yang, B., Wu, Y.J., Zhu, M., Fan, S.B., Lin, J., Zhang, K., et al.: Identification of cross-linked peptides from complex samples. Nature methods. 9, 904-906 (2012)

14. Konijnenberg, A., Butterer, A., Sobott, F.: Native ion mobility-mass spectrometry and related methods in structural biology. Biochimica et biophysica acta. 1834, 1239-1256 (2013)

15. Savvides, S.N., Yeo, H.-Y., Beck, M.R., Blaesing, F., Lurz, R., Lanka, et al.: VirB11 ATPases are dynamic hexameric assemblies: new insights into bacterial type IV secretion. EMBO J. 22, 1969-2980 (2003)

16. Hopper, J.T., Oldham, N.J.: Collision induced unfolding of protein ions in the gas phase studied by ion mobility-mass spectrometry: the effect of ligand binding on conformational stability. Journal of the American Society for Mass Spectrometry. 20, 1851-1858 (2009)

17. Hyung, S.J., Robinson, C.V., Ruotolo, B.T.: Gas-phase unfolding and disassembly reveals stability differences in ligand-bound multiprotein complexes. Chemistry & biology. 16, 382-390 (2009)

18. Zhou, M., Politis, A., Davies, R., Liko, I, Wu, K.-J., Stewart, A.G. et al.: Ion mobility mass spectrometry of a rotary ATPase reveals ATP-induced reduction in conformational flexibility. Nature Chem. 6, 208-245 (2014)

19. Black, D.S., Irwin, B., Moyed, H.S.: Autoregulation of hip, an operon that affects lethality due to inhibition of peptidoglycan or DNA synthesis. Journal of bacteriology. 176, 4081-4091 (1994)

20. Leitner, A., Joachimiak, L.A., Bracher, A., Monkemeyer, L., Walzthoeni, T., Chen, B., et al.: The molecular architecture of the eukaryotic chaperonin TRiC/CCT. Structure. 20, 814-825 (2012)

21. Walzthoeni, T., Claassen, M., Leitner, A., Herzog, F., Bohn, S., Forster, F., et al.: False discovery rate estimation for cross-linked peptides identified by mass spectrometry. Nature methods. 9, 901-903 (2012)

22. De Gieter, S., Konijnenberg, A., Talavera, A., Butterer, A., Haesaerts, S., De Greve, H., et al.: The intrinsically disordered domain of the antitoxin Phd chaperones the toxin Doc against irreversible inactivation and misfolding. The Journal of biological chemistry. 289, 34013-34023 (2014)

23. Pacholarz, K.J., Garlish, R.A., Taylor, R.J., Barran, P.E.: Mass spectrometry based tools to investigate protein-ligand interactions for drug discovery. Chemical Society reviews. 41, 4335-4355 (2012)

24. **Niu, S., Rabuck, J.N., Ruotolo, B.T.: Ion mobility-mass spectrometry of intact protein--ligand complexes for pharmaceutical drug discovery and development. Current opinion in chemical biology. 17, 809-817 (2013)**

25. **Williams, J.J., Hergenrother, P.J.: Artificial activation of toxin-antitoxin systems as an antibacterial strategy. Trends in microbiology. 20, 291-298 (2012)**

26. **Shapiro, S.: Speculative strategies for new antibacterials: all roads should not lead to Rome. The Journal of antibiotics. 66, 371-386 (2013)**

27. **Wen, Y., Behiels, E., Devreese, B.: Toxin-Antitoxin systems: their role in persistence, biofilm formation, and pathogenicity. Pathogens and disease. 70, 240-249 (2014)**

Table 1 Experimental and theoretical collision cross section and molecular weight

	apoHipA	HipA ATP:Mg	pHipA	HipB2*	HipAB2 ATP:Mg	HipA2B2 ATP:Mg
Experimental CCS(Å²)#	4962 (186)	3822(34)	3744(125)	2629(70)	5249(152)	8116(14)
PA *S.O.* CCS(Å²)	No data	3628	3576	2585	5273	8143
PA *E.coli* CCS(Å²)	No data	3276	3160	2235	4366	6717
Experimental MW (Da)	50768±5	51336±63	50878±19	21839±1 25344±2	76659±33	127940±47
Theoretical MW (Da)	50764	51320	50844	21839 25341	76660	127980

*The two different experimental and theoretical molecular weights indicate the state with or without His tag. #The Experimental CCS is the average value generated from at least 3 replicate measurements. The value between brackets is the standard deviation

400

401

402 **Table 2 Crosslinked peptides between HipA and HipB assembly identified by pLink**

No.	Sequence 1(X-linked residue) X-linked position in sequence	Sequence 2(X-linked residue) X-linked position in sequence	pLink Score	Calc_M	Cα-Cα distance	Mass error (ppm)
1	IEDPTMWPMEIWDGKPR(15) HipA(143)	DVKDIR(3) HipA(264)	7.41E-04	2982.46	18.6 Å	0.30
2	RKSAALTQDVAAMLCGVTK(2) HipB(39)	KYER(1) HipA(252)	8.57E-02	2694.42	36.6 Å	0.62
3	VEKGEDVYISTVFK(3) HipB(64)	KTLIR(1) HipB(57)	9.95E-09	2380.33	10.6 Å	0.013
4	VYEDTLLETIMASPLNQQSLGLLIKER(25) HipB(35)	VEKGEDVYISTVFK(3) HipB(64)	4.36E-02	4824.55	28.2 Å	1.27
5	VEKGEDVYISTVFK(3) HipB(64)	GSHMNGTDIK(1) HipB(-2°)	9.56E-02	2809.384	ND*	-4.66
6	VYEDTLLETIMASPLNQQSLGLLIKER(25) HipB(35)	GSHMNGTDIK(1) HipB(-2°)	8.44E-01	4270.18	ND*	-0.89

403 *No density of HipB in the crystal structure because of its flexibility.

404 ° Cross linked at amino terminus, -2 refers to the fact that HipB was produced as a recombinant
405 protein with HisTag. The actual start of the protein is at His.

406

Figure Legends:

Figure 1. IM-MS analysis of recombinant HipA. **a.** Native mass spectrum and drift time vs m/z plot of a freshly prepared HipA sample. The plot displays two distinct populations, i.e. apoHipA and phosphorylated HipA (pHipA). The two populations that separated in the gas phase are encircled. **b.** Native mass spectrum and drift time vs m/z plot of a sample containing only nonphosphorylated HipA alone (apoHipA). **c.** Drift time profiles of the 13+ ion of pHipA and apoHipA respectively. Calculation of the collision cross section indicated a value of 3800Å^2 for pHipA and 4750Å^2 apoHipA, respectively. **d.** Native mass spectrum and drift time vs m/z plot of holoHipA regard to ATP Mg2+ bound HipA. The drift time of holoHipA (Green) was shown to be more corresponding to the pHipA than of apoHipA. The dimer population of Mg^{2+}-ATP bound HipA (Black) could reflect the transient interaction necessary to perform the intermolecular autophosphorylation. **e.** Schematic view of the three different HipA conformations. Upon binding of ATP and Mg^{2+}, apoHipA is phosphorylated transforming the protein to a more compact pHipA conformation.

Figure 2. IM-MS characterization of HipA-HipB assembly. a. IM-MS measurement of the ATP-Mg^{2+} bound HipA complexed with HipB. Both the electrospray spectrum and **b.** the drift time vs m/z-drift time view are shown, the charges of the 4 populations are denoted (A: ATP-Mg^{2+} bound HipA B: $HipB_2$, , C: ATP-Mg^{2+} bound $HipAB_2$, D: ATP-Mg^{2+} bound $HipA_2B_2$). The 4 populations are also circled in the m/z-drift time view. **c.** Native ESI-MS spectrum of $HipB_2$DNA complex. **d.** Plot of experimental and theoretical PA model CCS vs molecular weight of $HipB_2$, HipA, $HipAB_2$ and $HipA_2B_2$.

Figure 3. Cross-linking the HipAB complex with BS-3. a. The crosslinked peptides are denoted on the *S.oneidensis* MR-1 $HipA_2B_2$ 3D dimensional structure accompanied with the distance restraints. The structural model of *S.oneidensis* MR-1 $HipA_2B_2$ was generated from

PDB: 4PU3 **b** MS/MS spectrum of the pHipA crosslinked peptide containing K143 and K264, displayed in the output generated from pLink. **c.** Three dimensional structures of pHipA and HipA, binding the ATP mimicking AMPNP. The distances between K143 and K 264 are 18.6Å and 40.3Å respectively indicating that in the AMPPNP bound HipA, the distance between these residues is too large and crosslinking is further hindered by a helical structure. The observation of the crosslinked K143 and K264 in the pHipA thus reflects the pLoop ejection upon of HipA phosphorylation. The atomic structure representation of *S.oneidensis* MR-1 HipA and pHipA were generated from PDB: 4PU3 and 4PU5.

Supplementary information

Table S1. Experimental CCS values obtained from replicate experiments of the different complexes.

Figure S1. Denatured Myoglobin CCS calibration curve generated from Driftscope.

Figure S2. Native mass spectrum of HipB indicated HipB exists in dimeric form.

Figure S3. MS/MS spectrum of the crosslinked peptide containing K143 and K264 in pHipA screened from pLink and reanalyzed by xlink.

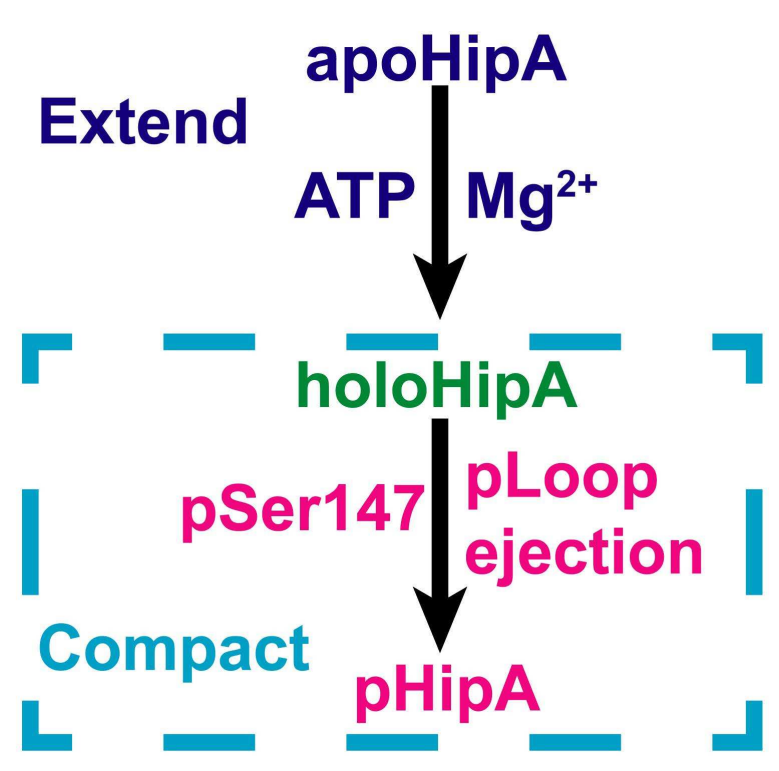
apoHipA
Extend
ATP
Mg2+
holoHipA
pSer147
pLoop
ejection
Compact
pHipA

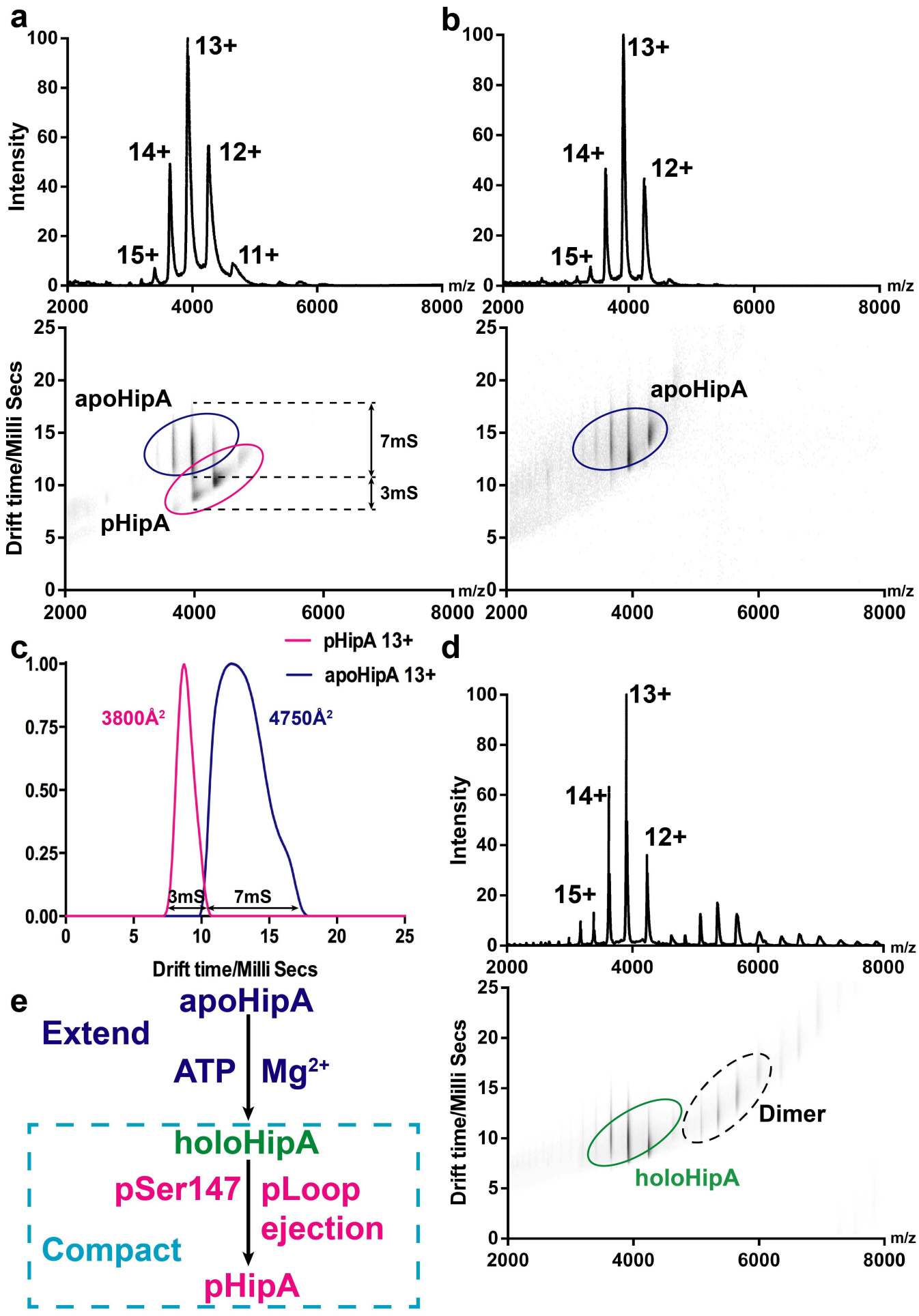
a
b
Intensity
13+
14+
12+
15+
11+
m/z
2000
4000
6000
8000
Drift time/Milli Secs
apoHipA
pHipA
7mS
3mS
c
pHipA 13+
apoHipA 13+
3800Å²
4750Å²
3mS
7mS
d
e
apoHipA
Extend
ATP
Mg2+
holoHipA
pSer147
pLoop
ejection
Compact
pHipA
Dimer

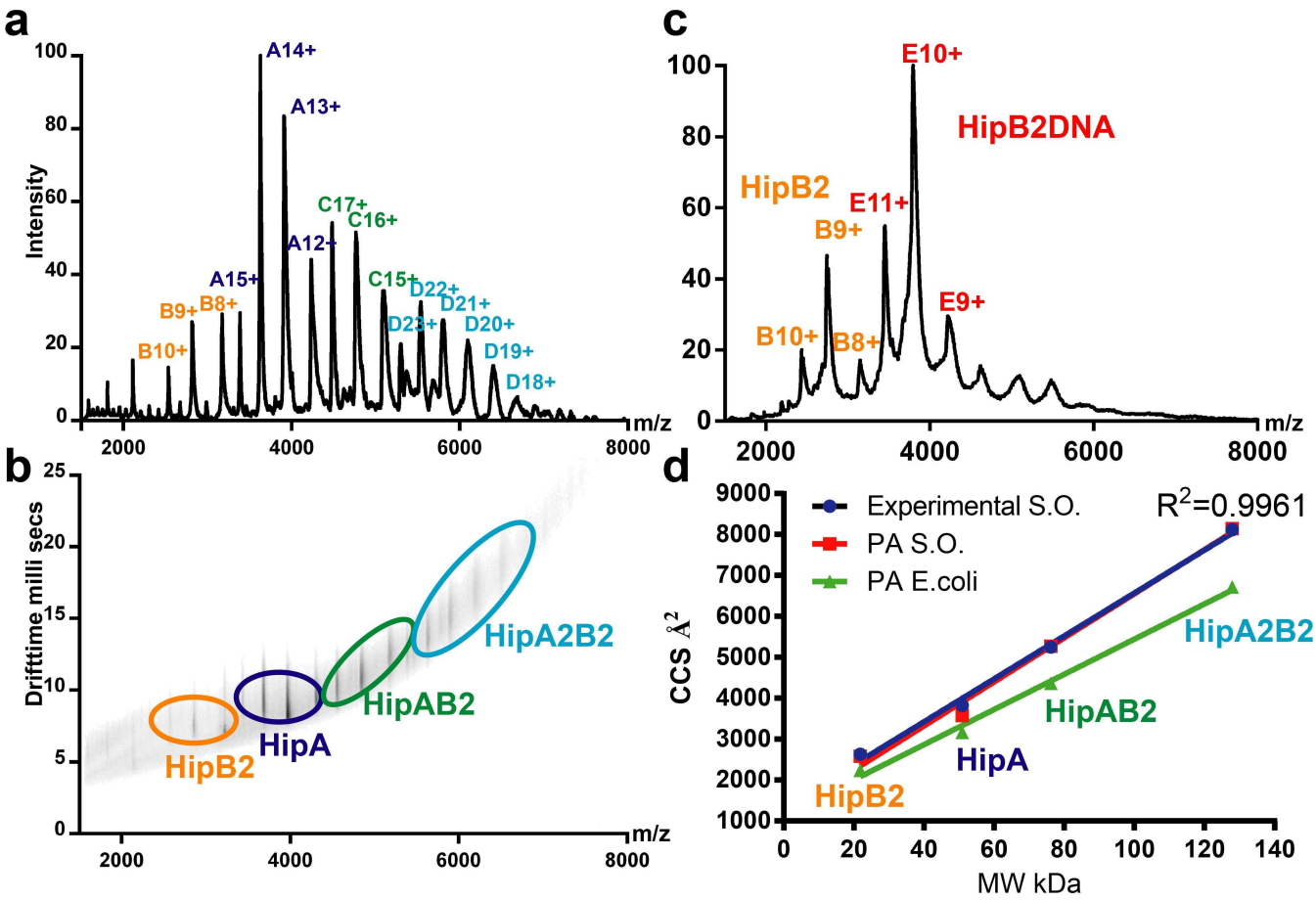
a
Intensity
m/z
A14+
A13+
A12+
A15+
C17+
C16+
C15+
D22+
D21+
D23+
D20+
D19+
D18+
B9+
B8+
B10+
b
Drifttime milli secs
m/z
HipA2B2
HipAB2
HipA
HipB2
c
HipB2DNA
E10+
E11+
E9+
B9+
B8+
B10+
HipB2
m/z
d
CCS Å2
MW kDa
Experimental S.O.
PA S.O.
PA E.coli
R2=0.9961
HipA2B2
HipAB2
HipA
HipB2

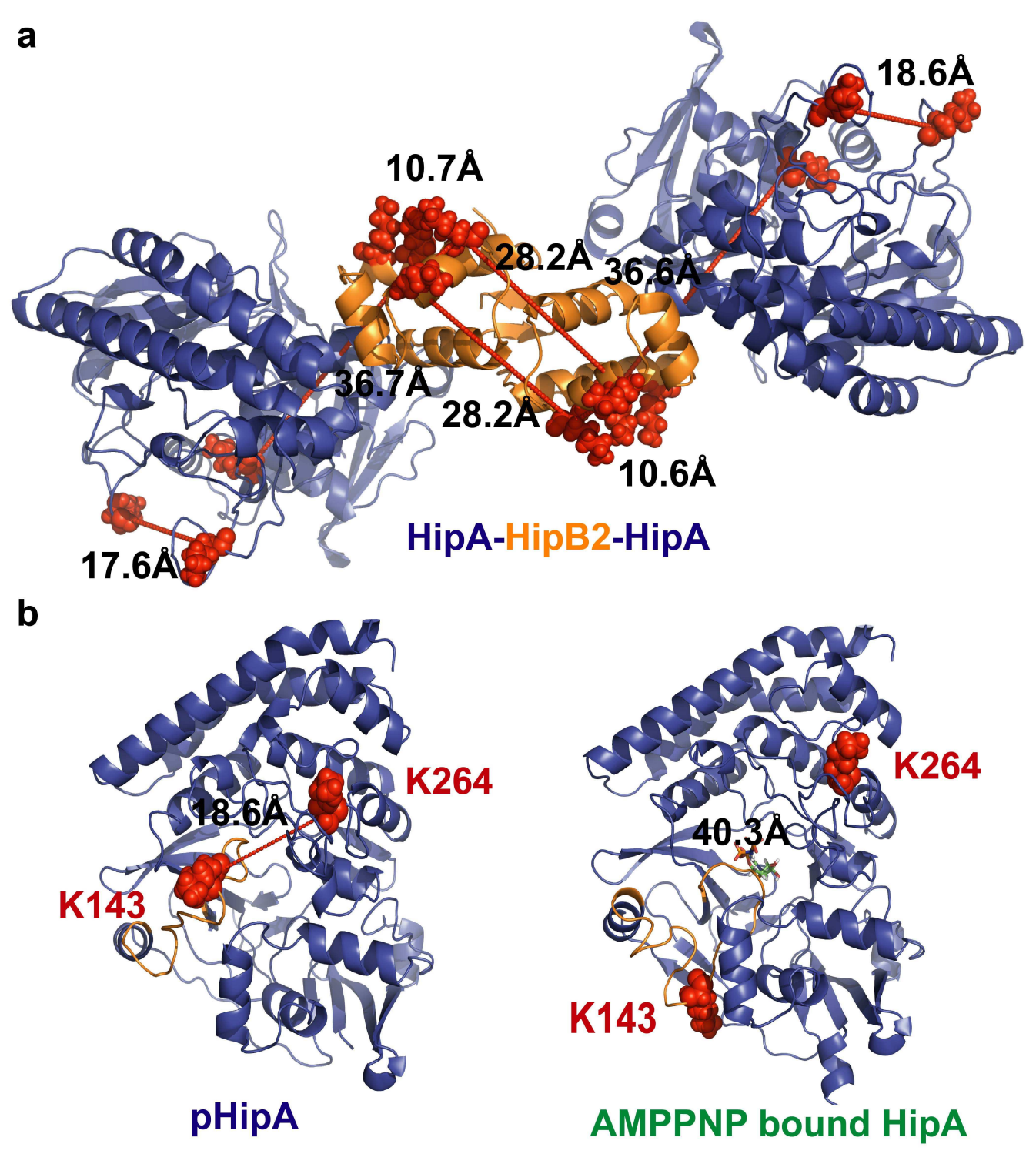
a
18.6Å
10.7Å
28.2Å
36.6Å
36.7Å
28.2Å
10.6Å
17.6Å
HipA-HipB2-HipA
b
K264
18.6Å
K143
pHipA
K264
40.3Å
K143
AMPPNP bound HipA

Table S1. Replicate measurement of the CCS supplemented to Table 1. The CCS value shown in Table 1 is the average of 3 or 4 measurements in the same IM parameters.

Experimental CCS ($Å^2$)	1st	2nd	3rd	4th	Average	Standard deviation
apoHipA	4820	4751	5216	5060	4962	186
HipA ATP:Mg	3800	3836	3882		3822	34
pHipA	3610	3817	3638	3910	3744	125
HipB2	2596	2565	2726		2629	70
HipAB2 ATP:Mg	5150	5464	5132		5249	152
HipA2B2 ATP:Mg	8106	8105	8136		8116	14

Table S1. Replicate measurement of the CCS supplemented to Table 1. The CCS value shown in Table 1 is the average of 3 or 4 measurements in the same IM parameters.

Experimental CCS ($Å^2$)	1st	2nd	3rd	4th	Average	Standard deviation
apoHipA	4820	4751	5216	5060	4962	186
HipA ATP:Mg	3800	3836	3882		3822	34
pHipA	3610	3817	3638	3910	3744	125
HipB2	2596	2565	2726		2629	70
HipAB2 ATP:Mg	5150	5464	5132		5249	152
HipA2B2 ATP:Mg	8106	8105	8136		8116	14